

An exact analysis of radiation absorption and Dufour effect on MHD convective flow of Cu-water nanofluid with heat generation and chemical reaction

Rajdeep Bordoloi^{*,‡}, Dipunja Gohain^{*§}, Nazibuddin Ahmed^{*¶} and Ali J. Chamkha^{†||}

**Department of Mathematics,
Gauhati University,
Guwahati-781014, India*

*†Faculty of Engineering,
Kuwait College of Science & Technology,*

Doha District, 35004 Kuwait

‡rajdeepbordoloi24@gmail.com

§dipunjagohain44@gmail.com

¶nazib@gauhati.ac.in

||achamkha@yahoo.com

Received 18 March 2023

Revised 22 May 2023

Accepted 9 July 2023

Published 4 October 2023

The combined effects of diffusion-thermo and radiative absorption on free convective hydro-magnetic heat-generating chemically reactive flow of Cu-water nanofluid past an instantaneously accelerated unlimited vertical plate nested in a porous medium are investigated. A comparative analysis is executed for both isothermal and ramped conditions. The set of transformed domain equations has been obtained using a closed form of the Laplace transform method with the help of the Heaviside step function. Graphical and tabular explanations are provided for the physical characteristics of several flow parameters affecting the problem. Graphs are generated using MATLAB computing software. Findings of the problem manifest that the diffusion-thermo parameter and the radiation absorption parameter intensify the velocity and fluid temperature in the entire fluid area. This augmentation is most prominent for copper nanoparticles. Concentration, temperature, and velocity profiles in the case of ramped conditions are less than in isothermal conditions. Furthermore, the ramped parameter amplifies the heat transfer rate while reversing the mass transfer rate. It is also established that the volume concentration of nanoparticles enhances the heat transfer rate. The present study is of great interest in numerous fields of industry and machine-building applications.

Keywords: Heat generation; radiation absorption; ramped effect; nanofluid; porous media; chemical reaction.

PACS numbers: 44.25.+f, 44.40.+a, 47.56.+r, 47.70.Fw, 52.30.Cv

[‡]Corresponding author.

1. Introduction

The intensification of heat transfer in thermal systems is a major obstacle due to the poor availability of energy sources. In today's high-energy power devices, efficient cooling solutions are absolutely needed. The low thermal properties of conventional fluids such as ethylene glycol, water, and motor oil make them inefficient heat transmission mediums. Hence, new technologies capable of improving the heat transfer properties of cooling fluid are trending among researchers. Nanometer-sized particles, such as metallic and non-metallic particles, can be used to improve heat conductivity by dispersing them in the typical fluid. Fluids having nanoparticles scattered in an ordinary liquid are known as nanofluids, as Choi¹ suggested in 1995. Nanofluids have a good deal of thermal conductivity than other normal fluids, so they can be used as a much better alternative than any other ordinary fluid. Numerous researchers worked both theoretically and experimentally to intensify the heat transfer of nanofluids. A few of them are Ahmed *et al.*,² Buongiorno,³ Das *et al.*,⁴ Liu *et al.*,⁵ Eastman *et al.*,⁶ Wang *et al.*,⁷ and Lee *et al.*⁸

In science and technology, interest among researchers in the field of excitatory heat transfer of nanofluids is extremely critical. It's because of the wide range of applications in the replication of cooling equipment for microelectronic and electronic appliances, solar energy, anthropology, etc. Because of the notable applications in industrial science and intense thermal property of nonfluid flows, a large number of researchers have shown their zeal to work on its flow characteristics over the last few decades. Some of the relevant works are Wen and Ding,⁹ Hamad *et al.*,¹⁰ Das and Jana,¹¹ Seth and Mishra,¹² Krishna *et al.*,¹³ Prasad *et al.*,¹⁴ Mahanthesh *et al.*,¹⁵ Chamkha and Aly,¹⁶ Turkyilmazoglu and Pop,¹⁷ Sheikholeslami *et al.*,¹⁸ etc.

When heat and mass are being transported together in fluid motion, then the relationship between driving potentials and fluxes is of a particularly complicated nature. Both the temperature gradient and the concentration gradient are seen to cause energy flux. The transport of heat through a concentration gradient is known as the Dufour effect. The applications of the Dufour effect are momentous in solar collectors, reactor safety, nuclear waste disposal, petrology, hydrology, etc. Ahamad *et al.*,¹⁹ Reddy and Chamkha,²⁰ Hayat *et al.*,²¹ Singha *et al.*,²² Waini *et al.*,²³ and Pal *et al.*²⁴ are some recent works that show the importance of the Dufour effect.

Applications of ramped wall temperature and ramped velocity have become of great significance in modern technology. For example, ramped velocity is significant in measuring heart function, diagnosis of cardiovascular diseases, determining treatment, and making prognoses related to treadmill tests and ergometry, etc. Similarly, the ramped temperature is used in the phenomenon of nuclear-powered heat transfer control, heat transfer in buildings, heat transfer in turbine blades, and so on. The idea of working simultaneously with ramped plate velocity and ramped wall temperature was first introduced by Ahmed and Dutta²⁵ for Newtonian fluid over a suddenly started vertical plate. Anwar *et al.*²⁶ examined the impact of ramped

velocity and ramped temperature on free convective hydromagnetic flow for different nanofluids.

Recently, Abdelsalam *et al.*²⁷ theoretically investigated the physical traits of electro-magneto-hydrodynamics (EMHD) of blood stream for a hybrid fractional second-grade nanofluid. They concluded that heat transfer is higher for hybrid nanofluid than that of nanofluid. Mekheimer *et al.*²⁸ studied the two-dimensional flow of an incompressible fluid induced by a sinusoidal peristaltic wavy moving wall for a large Reynolds number. Mekheimer *et al.*²⁹ studied the slip effect with Hall current on the flow induced by sinusoidal peristaltic wavy wall through a porous medium. Idrissi *et al.*³⁰ investigated two-phase water hammer flows by applying Godunov methods numerically. Zeidan *et al.*³¹ presented a solution to the Reimann problem for the drift-flux model with modified Chaplygin two-phase flows. Zeidan *et al.*³² studied Aerogel numerically using two-phase flow equations system. Sharma *et al.*³³ studied the combined effect of thermophoresis and Brownian motion on MHD mixed convective flow. Shahid *et al.*³⁴ examined the physical features of magneto-hydrodynamics (MHD) Carreau nanofluid bi-convection flow past an upper paraboloid porous surface.

Keeping in mind the aforementioned peculiar findings and applications, the present study is dedicated to examining the influence of the Dufour effect and radiation absorption on hydromagnetic convective nanofluid flow across a suddenly moving infinite upright plate nestled in a porous medium with heat generation and chemical reaction. As far as the author's knowledge and literature survey, the ramped parameter has not yet been taken into account when dealing with nanofluids, but this investigation makes good use of it to scrutinize thermal as well as solutal convection. At the same time, ramped plate velocity and ramped temperature have been considered simultaneously. The current problem is unique in that it investigates the heat and mass transfer behavior of Cu-water nanofluid flow under the influence of volume concentration of nanoparticles, Dufour effect, radiation absorption, and ramped effect using Cogley *et al.*'s³⁵ model.

2. Basic Equations

Equations which describe the unsteady, incompressible natural MHD convective flow in the existence of diffusion-thermo effect, heat generation, and radiation absorption subject to Boussinesq's approximation are given as

Equation of continuity,

$$\nabla \cdot \mathbf{q} = 0. \quad (1)$$

Momentum equation,

$$\rho \left[\frac{\partial \mathbf{q}}{\partial t} + (\mathbf{q} \cdot \nabla) \mathbf{q} \right] = \mu \nabla^2 \mathbf{q} + \mathbf{J} \times \mathbf{B} + \rho \mathbf{g} \beta (T - T_\infty) + \rho \mathbf{g} \bar{\beta} (C - C_\infty) - \frac{\mu}{k} \mathbf{q}. \quad (2)$$

Energy equation,

$$\rho C_p \left[\frac{\partial T}{\partial t} + (\mathbf{q} \cdot \nabla) T \right] = \kappa \nabla^2 T - \nabla \cdot \mathbf{q}_r + \frac{\rho D_M K_T}{C_s} \nabla^2 C + \bar{Q}(T - T_\infty) + Q_l^*(C - C_\infty). \quad (3)$$

Species continuity equation,

$$\frac{\partial C}{\partial t} + (\mathbf{q} \cdot \nabla) C = D_M \nabla^2 C - K^*(C - C_\infty). \quad (4)$$

Ohm's law for moving conductor,

$$\mathbf{J} = \sigma(\mathbf{E} + \mathbf{q} \times \mathbf{B}). \quad (5)$$

3. Formulation and Solution

Consider an unsteady, viscous, incompressible, hydromagnetic free convective heat-generating nanofluid flow past an infinitely long vertical plate nestled in a porous medium as pictured in Fig. 1. The X-axis runs parallel to the plate through which fluid flow is presumed, and the Y-axis is normal to the X-axis. B_0 and q_r be the strength of the uniform magnetic field and radiative heat flux, respectively, applied along the Y-direction.

The following assumptions have been considered for the flow problem,

- Entire fluid properties are constant except for the density in the body force term.
- No electric field is applied externally.
- The shape and size of the nanoparticles are consistent.
- The base fluid and nanoparticles are in thermal equilibrium.

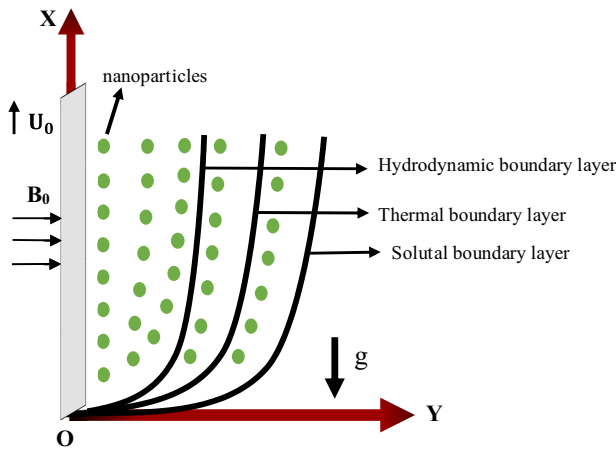


Fig. 1. (Color online) Geometrical layout.

Under these assumptions and Boussinesq's approximation, the governing equations for the flow problem are given by³⁶

$$\rho_{nf} \frac{\partial u'}{\partial \bar{t}} = \mu_{nf} \frac{\partial^2 u'}{\partial \bar{y}^2} - \sigma_{nf} B_0^2 u' + g(\rho\beta)_{nf}(T - T_\infty) + g(\rho\beta_c)_{nf}(C - C_\infty) - \frac{\mu_{nf}}{K} u', \quad (6)$$

$$(\rho C_p)_{nf} \frac{\partial T}{\partial \bar{t}} = \kappa_{nf} \frac{\partial^2 T}{\partial \bar{y}^2} - \frac{\partial q_r}{\partial \bar{y}} + \frac{D_M K_T}{C_s} \frac{\partial^2 C}{\partial \bar{y}^2} + Q_0(T - T_\infty) + Q_i^*(C - C_\infty), \quad (7)$$

$$\frac{\partial C}{\partial \bar{t}} = D_1 \frac{\partial^2 C}{\partial \bar{y}^2} - k_r(C - C_\infty). \quad (8)$$

Initially, the fluid was at rest at a constant temperature T_∞ and fixed concentration C_∞ . Suddenly, the plate starts to move with temporary acceleration $\frac{U_0}{t_0}$ and the fluid temperature rises linearly about the steady mean T_∞ . For $\bar{t} > t_0$, the plate starts to move uniformly and fluid acceleration and concentration attain fixed values T_w and C_w . The fluid far away from the plate is not disturbed due to the sudden motion of the plate (see Ref. 26).

The corresponding initial and boundary conditions are given by,²⁶

$$\left. \begin{aligned} u' &= 0, \quad T = T_\infty, \quad C = C_\infty, \quad \forall \bar{y} \geq 0, \quad \bar{t} \leq 0, \\ u' &= U_0 \frac{\bar{t}}{t_0}, \quad T = T_\infty + (T_w - T_\infty) \frac{\bar{t}}{t_0}, \quad C = C_w, \quad 0 < \bar{t} \leq t_0 \quad \text{for } \bar{y} = 0, \\ u' &= U_0, \quad T = T_w, \quad C = C_w, \quad \bar{t} > t_0, \quad \text{for } \bar{y} = 0, \\ u' &\rightarrow 0, \quad T \rightarrow T_\infty, \quad C \rightarrow C_\infty, \quad \text{as } \bar{y} \rightarrow \infty, \quad \forall \bar{t} \geq 0. \end{aligned} \right\} \quad (9)$$

By Cogley's model,³⁵ the radiative heat flux q_r for an optically thin non-gray gas is defined by the relation,

$$\begin{aligned} \frac{\partial q_r}{\partial \bar{y}} &= 4(T - T_\infty) \int_0^\infty (K_\lambda)_0 \left(\frac{\partial e_{\lambda h}}{\partial T} \right)_0 d\lambda, \\ &= 4I(T - T_\infty), \quad \text{where, } I = \int_0^\infty (K_\lambda)_0 \left(\frac{\partial e_{\lambda h}}{\partial T} \right)_0 d\lambda, \end{aligned} \quad (10)$$

where K_λ , $e_{\lambda h}$, and λ are absorption coefficient, Planck's function, and wavelength, respectively.

Utilizing the Eqs. (10) and (7) reduces to

$$\begin{aligned} (\rho C_p)_{nf} \frac{\partial T}{\partial \bar{t}} &= \kappa_{nf} \frac{\partial^2 T}{\partial \bar{y}^2} - 4I(T - T_\infty) + \frac{D_M K_T}{C_s} \frac{\partial^2 C}{\partial \bar{y}^2} \\ &+ Q_0(T - T_\infty) + Q_i^*(C - C_\infty). \end{aligned} \quad (11)$$

The expressions for various thermo-physical features of nanofluids are given by

$$\mu_{nf} = \frac{\mu_f}{(1 - \varphi)^{2.5}}, \quad \rho_{nf} = \rho_f \left[1 - \varphi + \varphi \frac{\rho_{np}}{\rho_f} \right], \quad \sigma = \frac{\sigma_{np}}{\sigma_f},$$

$$\begin{aligned}
 (\rho C_p)_{nf} &= (\rho C_p)_f \left[1 - \varphi + \varphi \frac{(\rho C_p)_{np}}{(\rho C_p)_f} \right], & \sigma_{nf} &= \sigma_f \left(1 + \frac{3(\sigma - 1)\varphi}{\sigma + 2 - (\sigma - 1)\varphi} \right), \\
 (\rho\beta)_{nf} &= (\rho\beta)_f \left[1 - \varphi + \varphi \frac{\rho\beta_{np}}{(\rho\beta)_f} \right], & (\rho\beta_c)_{nf} &= (\rho\beta_c)_f \left[1 - \varphi + \varphi \frac{(\rho\beta_c)_{np}}{(\rho\beta_c)_f} \right].
 \end{aligned}
 \tag{12}$$

Hamilton and Crosser’s model is used in this study to efficiently predict the thermal conductivity of nanoparticles.

$$\frac{\kappa_{nf}}{\kappa_f} = \frac{\kappa_{np} + 2\kappa_f - 2(\kappa_f - \kappa_{np})\varphi}{\kappa_{np} + 2\kappa_f + \varphi(\kappa_f - \kappa_{np})}.
 \tag{13}$$

We introduce some dimensionless variables and parameters:

$$\begin{aligned}
 y &= \frac{U_0 \bar{y}}{\nu_f}, & u &= \frac{u'}{U_0}, & t &= \frac{\bar{t}}{t_0}, & Ra &= \frac{U_0^2 t_0}{\nu_f}, & \theta &= \frac{T - T_\infty}{T_w - T_\infty}, & \phi &= \frac{C - C_\infty}{C_w - C_\infty}, \\
 M &= \frac{\sigma_f B_0^2 \nu_f}{\rho_f U_0^2}, & N &= \frac{4I \nu_f}{U_0^2 (\rho C_p)_f}, & Pr &= \frac{(\mu C_p)_f}{\kappa_f}, & Q &= \frac{Q_0 \nu_f}{U_0^2 (\rho C_p)_f}, \\
 Gr &= \frac{g(\nu\beta)_f (T_w - T_\infty)}{U_0^3}, & Gm &= \frac{g(\nu\beta_c)_f (C_w - C_\infty)}{U_0^3}, & Q_l &= \frac{Q_l^* \nu_f (C_w - C_\infty)}{U_0^2 (\rho C_p)_f (T_w - T_\infty)}, \\
 K &= \frac{\bar{K} U_0^2}{\nu_f^2}, & k &= \frac{k_r \nu_f}{U_0^2}, & Sc &= \frac{\nu_f}{D_1}, & Du &= \frac{D_M K_T (C_w - C_\infty)}{\kappa_f C_s (T_w - T_\infty)}.
 \end{aligned}$$

Employing above non-dimensional variables and parameters together with Eqs. (12) and (13), Eqs. (6), (11) and (8) gets transformed into the following dimensionless form:

$$\frac{\partial^2 u}{\partial y^2} - \lambda_1 \frac{\partial u}{\partial t} - \lambda_4 u = -\lambda_2 Gr \theta - \lambda_3 Gm \phi,
 \tag{14}$$

$$\frac{\partial^2 \theta}{\partial y^2} - \alpha_1 \frac{\partial \theta}{\partial t} + (\alpha_4 - \alpha_2) \theta = -\alpha_3 \frac{\partial^2 \phi}{\partial y^2} - \alpha_5 \phi,
 \tag{15}$$

$$\frac{\partial^2 \phi}{\partial y^2} - \xi_1 \frac{\partial \phi}{\partial t} - \xi_2 \phi = 0,
 \tag{16}$$

where

$$\begin{aligned}
 \varphi_1 &= \frac{1}{(1 - \varphi)^{2.5}}, & \varphi_2 &= 1 - \varphi + \varphi \frac{(\rho C_p)_{np}}{(\rho C_p)_f}, & \varphi_4 &= 1 - \varphi + \varphi \frac{(\rho\beta_c)_{np}}{(\rho\beta_c)_f}, \\
 \varphi_5 &= 1 - \varphi + \varphi \frac{\rho_{np}}{\rho_f}, & \varphi_6 &= 1 + \frac{3(\sigma - 1)\varphi}{\sigma + 2 - (\sigma - 1)\varphi}, & \varphi_7 &= \frac{\kappa_{np} + 2\kappa_f - 2(\kappa_f - \kappa_{np})\varphi}{\kappa_{np} + 2\kappa_f + \varphi(\kappa_f - \kappa_{np})}, \\
 \lambda_1 &= \frac{\varphi_5}{\varphi_1 Ra}, & \lambda_2 &= \frac{\varphi_3}{\varphi_1}, & \lambda_3 &= \frac{\varphi_4}{\varphi_1}, & \lambda_4 &= \frac{\varphi_6}{\varphi_1} M + \frac{1}{K}, & \alpha_1 &= \frac{\varphi_2}{\varphi_7} Pr, & \alpha_2 &= \frac{N Pr}{\varphi_7}, \\
 \alpha_3 &= \frac{Du}{\varphi_7}, & \alpha_4 &= \frac{Q Pr}{\varphi_7}, & \alpha_5 &= \frac{Q_l Pr}{\varphi_7}, & \xi_1 &= \frac{Sc}{Ra}, & \xi_2 &= k Sc.
 \end{aligned}$$

Non-dimensional form of the boundary conditions (9) is

$$\begin{aligned}
 u &= 0, & \theta &= 0, & \phi &= 0, & \forall y \geq 0, & t \leq 0, \\
 u &= t, & \theta &= t, & \phi &= 1, & \text{at } 0 < t \leq 1 & \text{ for } y = 0, \\
 u &= 1, & \theta &= 1, & \phi &= 1, & \text{at } t > 1 & \text{ for } y = 0, \\
 u &\rightarrow 0, & \theta &\rightarrow 0, & \phi &\rightarrow 0, & \text{as } y \rightarrow \infty, & \forall t \geq 0.
 \end{aligned}
 \tag{17}$$

4. Solution Procedure

After implementing the Laplace transform technique, Eqs. (14)–(16) and boundary conditions (17) are transformed to

$$\frac{d^2 \bar{u}}{dy^2} - \lambda_1(s + \lambda_5) \bar{u} = -\lambda_2 Gr \bar{\theta} - \lambda_3 Gm \bar{\phi},
 \tag{18}$$

$$\frac{d^2 \bar{\theta}}{dy^2} - \alpha_1(s + \xi_3) \bar{\theta} = -\alpha_3 \frac{d^2 \bar{\phi}}{dy^2} - \alpha_5 \bar{\phi},
 \tag{19}$$

$$\frac{d^2 \bar{\phi}}{dy^2} - \xi_1(s + \xi_2) \bar{\phi} = 0.
 \tag{20}$$

The relevant boundary conditions are

$$\begin{aligned}
 \bar{u} &= \bar{\theta} = \frac{1 - e^{-s}}{s^2}, & \bar{\phi} &= \frac{1}{s} & \text{at } y = 0, \\
 \bar{u} &\rightarrow 0, & \bar{\theta} &\rightarrow 0, & \bar{\phi} &\rightarrow 0 & \text{as } y \rightarrow \infty,
 \end{aligned}
 \tag{21}$$

where,

$$\lambda_5 = \frac{\lambda_4}{\lambda_1}, \quad \xi_3 = \frac{\alpha_2 - \alpha_4}{\alpha_1}.$$

The solutions of the Eqs. (18)–(20) under the condition (21) are obtained as follows:

$$\bar{\phi} = \frac{1}{s} e^{-y\sqrt{\xi_1}\sqrt{s+\xi_2}},
 \tag{22}$$

$$\begin{aligned}
 \bar{\theta} &= \frac{1 - e^{-s}}{s^2} e^{-y\sqrt{\alpha_1}\sqrt{s+\xi_3}} + \Lambda_2 \frac{(s + \xi_2)}{s(s + \Lambda_1)} e^{-y\sqrt{\alpha_1}\sqrt{s+\xi_3}} + \frac{\Lambda_3}{s(s + \Lambda_1)} e^{-y\sqrt{\alpha_1}\sqrt{s+\xi_3}} \\
 &\quad - \Lambda_2 \frac{(s + \xi_2)}{s(s + \Lambda_1)} e^{-y\sqrt{\xi_1}\sqrt{s+\xi_2}} - \frac{\Lambda_3}{s(s + \Lambda_1)} e^{-y\sqrt{\xi_1}\sqrt{s+\xi_2}},
 \end{aligned}
 \tag{23}$$

$$\begin{aligned}
 \bar{u} &= \Lambda_0 e^{-y\sqrt{\lambda_1}\sqrt{s+\lambda_5}} + \Lambda_5 \frac{1 - e^{-s}}{s^2(s + \Lambda_4)} e^{-y\sqrt{\alpha_1}\sqrt{s+\xi_3}} \\
 &\quad + \Lambda_6 \frac{s + \xi_2}{s(s + \Lambda_1)(s + \Lambda_4)} e^{-y\sqrt{\alpha_1}\sqrt{s+\xi_3}} + \Lambda_7 \frac{1}{s(s + \Lambda_1)(s + \Lambda_4)} e^{-y\sqrt{\alpha_1}\sqrt{s+\xi_3}} \\
 &\quad + \Lambda_8 \frac{s + \xi_2}{s(s + \Lambda_1)(s + \Lambda_9)} e^{-y\sqrt{\xi_1}\sqrt{s+\xi_2}} + \Lambda_{10} \frac{1}{s(s + \Lambda_1)(s + \Lambda_9)} e^{-y\sqrt{\xi_1}\sqrt{s+\xi_2}} \\
 &\quad + \Lambda_{11} \frac{1}{s(s + \Lambda_9)} e^{-y\sqrt{\xi_1}\sqrt{s+\xi_2}},
 \end{aligned}
 \tag{24}$$

where,

$$\begin{aligned} \Lambda_0 &= \frac{(1 - e^{-s})}{s^2} \left[1 - \frac{\Lambda_5}{s + \Lambda_4} \right] - \Lambda_6 \frac{s + \xi_2}{s(s + \Lambda_1)(s + \Lambda_4)} - \Lambda_7 \frac{1}{s(s + \Lambda_1)(s + \Lambda_4)} \\ &\quad - \Lambda_8 \frac{s + \xi_2}{s(s + \Lambda_1)(s + \Lambda_9)} - \Lambda_{10} \frac{1}{s(s + \Lambda_1)(s + \Lambda_9)} - \Lambda_{11} \frac{1}{s(s + \Lambda_9)}, \\ \Lambda_1 &= \frac{\xi_1 \xi_2 - \xi_3 \alpha_1}{\xi_1 - \alpha_1}, \quad \Lambda_2 = \frac{\xi_1 \alpha_3}{\xi_1 - \alpha_1}, \quad \Lambda_3 = \frac{\alpha_5}{\xi_1 - \alpha_1}, \quad \Lambda_4 = \frac{\alpha_1 \xi_3 - \lambda_1 \lambda_5}{\alpha_1 - \lambda_1}, \\ \Lambda_5 &= -\frac{\lambda_2 Gr}{\alpha_1 - \lambda_1}, \quad \Lambda_6 = -\frac{\lambda_2 Gr \Lambda_2}{\alpha_1 - \lambda_1}, \quad \Lambda_7 = -\frac{\lambda_2 Gr \Lambda_3}{\alpha_1 - \lambda_1}, \quad \Lambda_8 = \frac{\lambda_2 Gr \Lambda_2}{\xi_1 - \lambda_1}, \\ \Lambda_9 &= \frac{\xi_1 \xi_2 - \lambda_1 \lambda_5}{\xi_1 - \lambda_1}, \quad \Lambda_{10} = \frac{\lambda_2 Gr \Lambda_3}{\xi_1 - \lambda_1}, \quad \Lambda_{11} = -\frac{\lambda_3 Gm}{\xi_1 - \lambda_1}, \quad A_1 = \frac{\xi_2}{\Lambda_1}, \quad A_2 = \frac{\Lambda_1 - \xi_2}{\Lambda_1}, \\ A_3 &= \frac{1}{\Lambda_1}, \quad A_4 = -\frac{1}{\Lambda_1}, \quad A_5 = -\frac{1}{\Lambda_4^2}, \quad A_6 = -A_5, \quad A_7 = \frac{1}{\Lambda_4}, \quad A_8 = \frac{\xi_2}{\Lambda_1 \Lambda_4}, \\ A_9 &= \frac{\xi_2 - \Lambda_1}{\Lambda_1(\Lambda_1 - \Lambda_4)}, \quad A_{10} = \frac{\xi_2 - \Lambda_4}{\Lambda_4(\Lambda_4 - \Lambda_1)}, \quad A_{11} = \frac{1}{\Lambda_1 \Lambda_4}, \quad A_{12} = \frac{1}{\Lambda_1(\Lambda_1 - \Lambda_4)}, \\ A_{13} &= \frac{1}{\Lambda_4(\Lambda_4 - \Lambda_1)}, \quad A_{14} = \frac{\xi_2}{\Lambda_1 \Lambda_9}, \quad A_{15} = \frac{\xi_2 - \Lambda_1}{\Lambda_1(\Lambda_1 - \Lambda_9)}, \quad A_{16} = \frac{\xi_2 - \Lambda_9}{\Lambda_9(\Lambda_9 - \Lambda_1)}, \\ A_{17} &= \frac{1}{\Lambda_1 \Lambda_9}, \quad A_{18} = \frac{1}{\Lambda_1(\Lambda_1 - \Lambda_9)}, \quad A_{19} = \frac{1}{\Lambda_9(\Lambda_9 - \Lambda_1)}, \quad A_{20} = \frac{1}{\Lambda_9}, \quad A_{21} = -\frac{1}{\Lambda_9}. \end{aligned}$$

Now, employing inverse Laplace transformation on Eqs. (22)–(24), we get the following expressions for concentration, temperature profile, and velocity field:

$$\phi = \psi_1, \tag{25}$$

$$\theta = \theta_1 + \theta_2 + \theta_3 - \theta_4 - \theta_5, \tag{26}$$

$$u = \sum_{i=1}^7 u_i, \tag{27}$$

where

$$\begin{aligned} \theta_1 &= f_1 - \bar{f}_1, \quad \theta_2 = \Lambda_2[A_1\psi_2 + A_2\psi_3], \quad \theta_3 = \Lambda_3[A_3\psi_2 + A_4\psi_3], \\ \theta_4 &= \Lambda_2[A_1\psi_1 + A_2\psi_4], \quad \theta_5 = \Lambda_3[A_3\psi_1 + A_4\psi_4], \\ u_1 &= u_{1,1} - u_{1,2} - u_{1,3} - u_{1,4} - u_{1,5} - u_{1,6} - u_{1,7}, \quad u_{1,1} = f_2 - \bar{f}_2, \\ u_{1,2} &= \Lambda_5[A_5(\psi_5 - \bar{\psi}_5) + A_6(\psi_6 - \bar{\psi}_6) + A_7(f_2 - \bar{f}_2)], \\ u_{1,3} &= \Lambda_6[A_8\psi_5 + A_9\psi_7 + A_{10}\psi_6], \quad u_{1,4} = \Lambda_7[A_{11}\psi_5 + A_{12}\psi_7 + A_{13}\psi_6], \\ u_{1,5} &= \Lambda_8[A_{14}\psi_5 + A_{15}\psi_7 + A_{16}\psi_8], \quad u_{1,6} = \Lambda_{10}[A_{17}\psi_5 + A_{18}\psi_7 + A_{19}\psi_8], \\ u_{1,7} &= \Lambda_{11}[A_{20}\psi_5 + A_{21}\psi_8], \quad u_2 = \Lambda_5[A_5(\psi_2 - \bar{\psi}_2) + A_6(\psi_9 - \bar{\psi}_9) + A_7(f_1 - \bar{f}_1)], \\ u_3 &= \Lambda_6[A_8\psi_2 + A_9\psi_3 + A_{10}\psi_9], \quad u_4 = \Lambda_7[A_{11}\psi_2 + A_{12}\psi_3 + A_{13}\psi_9], \\ u_5 &= \Lambda_8[A_{14}\psi_1 + A_{15}\psi_4 + A_{16}\psi_{10}], \quad u_6 = \Lambda_{10}[A_{17}\psi_1 + A_{18}\psi_4 + A_{19}\psi_{10}], \\ u_7 &= \Lambda_{11}[A_{20}\psi_1 + A_{21}\psi_{10}], \quad f_1 = f(\alpha_1, \xi_3, y, t), \quad f_2 = f(\lambda_1, \lambda_5, y, t), \end{aligned}$$

$$\begin{aligned} \psi_1 &= \psi(\xi_1, \xi_2, y, t), & \psi_2 &= \psi(\alpha_1, \xi_3, y, t), & \psi_3 &= e^{-\Lambda_1 t} \psi(\alpha_1, \xi_3 - \Lambda_1, y, t), \\ \psi_4 &= e^{-\Lambda_1 t} \psi(\xi_1, \xi_2 - \Lambda_1, y, t), & \psi_5 &= \psi(\lambda_1, \lambda_5, y, t), \\ \psi_6 &= e^{-\Lambda_4 t} \psi(\lambda_1, \lambda_5 - \Lambda_4, y, t), & \psi_7 &= e^{-\Lambda_1 t} \psi(\lambda_1, \lambda_5 - \Lambda_1, y, t), \\ \psi_8 &= e^{-\Lambda_9 t} \psi(\lambda_1, \lambda_5 - \Lambda_9, y, t), & \psi_9 &= e^{-\Lambda_4 t} \psi(\alpha_1, \xi_3 - \Lambda_4, y, t), \\ \psi_{10} &= e^{-\Lambda_9 t} \psi(\xi_1, \xi_2 - \Lambda_9, y, t). \end{aligned}$$

The engineering quantities like drag force or skin friction coefficient (τ), Nusselt number/rate of heat transfer (Nu), and mass transfer/Sherwood number (Sh) at the plate in non-dimension form are derived as

$$\tau = -\varphi_1 \frac{\partial u}{\partial y} \Big|_{y=0}, \quad \text{Nu} = -\varphi_7 \frac{\partial \theta}{\partial y} \Big|_{y=0} \quad \text{and} \quad \text{Sh} = -\frac{\partial \phi}{\partial y} \Big|_{y=0}. \quad (28)$$

5. Parametric Study

Radiation absorption, as well as the diffusion-thermo effect on unsteady viscous incompressible MHD free convective heat-generating flow of nanofluid nested in a porous medium, is explored in the present study. To understand the physics behind the present problem, a parametric investigation is executed, and enumerated solutions are exposed with the help of graphs and tables. Impact of various physical parameters like absorption radiation parameter (Q_l), Dufour number (Du), Magnetic parameter (M), the volume fraction of nanoparticles (φ), chemical reaction (k), the permeability of porous media (K), Ramped parameter (Ra), and heat source (Q) on fluid velocity, concentration, and temperature together with Sherwood and Nusselt number are depicted graphically. It has been chosen that $\text{Pr} = 6.2$ (water) and $\text{Sc} = 0.6$ (for water vapor diffused in dry air) throughout the study. For graphical interpretation, water is considered as a base fluid and Cu (copper) as a nanoparticle. The thermophysical properties of water and copper are given in Table 1.

From Fig. 2, it is remarked that the fluid motion falls due to the enhanced volume concentration of nanoparticles (φ) for both isothermal ($t > 1$) and ramped ($t < 1$) cases. This is due to the frictional force created by the entrapment of nanoparticles in the base liquid, making the liquid denser and impeding its movement through the

Table 1. Thermophysical belongings of H₂O (Water) and Cu (Copper)(See Ref. 15).

Thermophysical features	Water	Copper
ρ (kg/m ³)	997.1	8933
C_p (J/kg.K)	4179	385
κ (W/mK)	0.613	401
$\beta \times 10^5$ (1/K)	21	1.67
$\beta_c \times 10^6$ (1/K)	298.2	3.05
σ (S/m)	5.5×10^{-6}	59.6×10^6

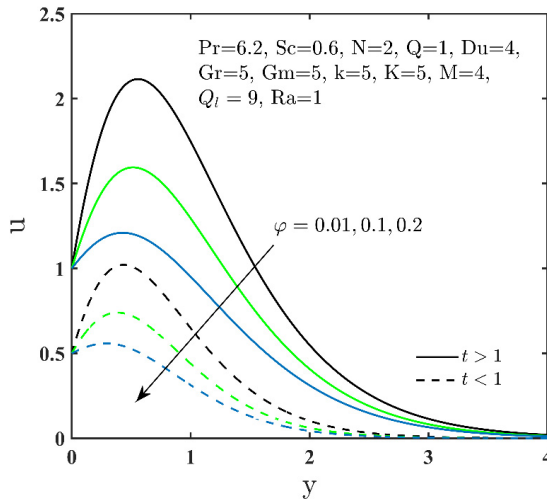


Fig. 2. (Color online) Velocity layout for φ .

porous medium. Figure 3 illustrates the impact of the diffusion-thermo parameter (Du) in the velocity field. It is seen that the Dufour parameter increases and so does the velocity distribution. It can be perceived that boundary layer thicknesses increase with an enhancement in Du .

A rise in the Dufour parameter improves the rate of transport through the boundary layer, thereby increasing the velocity in the fluid region. Figure 4 illustrates that fluid motion decelerates for an increased effect of magnetic field (M). The magnetic field creates a force named Lorentz force. This force is resistive in nature and also has a tendency to delay the fluid movement. This result perfectly follows the

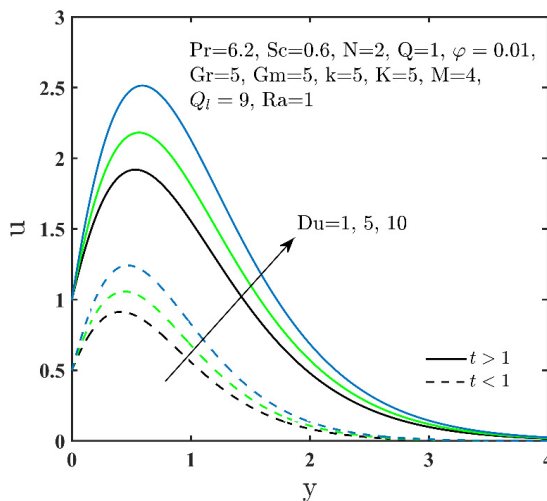


Fig. 3. (Color online) Velocity layout for Du .

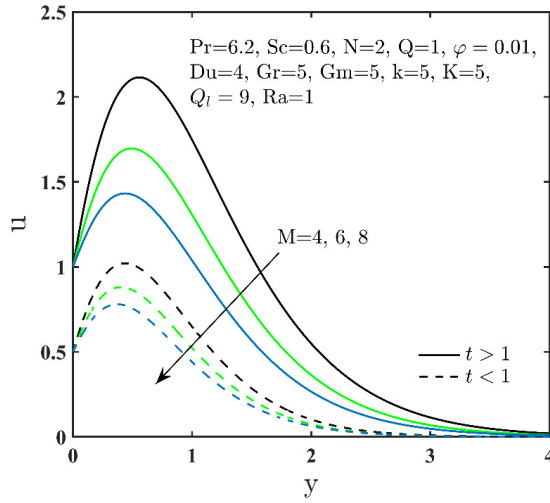


Fig. 4. (Color online) Velocity layout for M .

nature of the Lorentz force and also confirms that our solution is true. It is determined from Fig. 5 that velocity boosts up with the expansion of Q_l .

It can be figured out from Fig. 6 that the hydrodynamic boundary layer rises for increasing permeability parameter (K) for both the thermal conditions. Since higher permeability reduces the resistivity of the porous medium and henceforth hydrodynamic boundary layer increases. The consequence of ramped effect (Ra) on fluid motion is visualized in Fig. 7. Here the graph indicates that there is a proportional relationship between fluid velocity and ramped parameter (Ra). Increasing Ra means

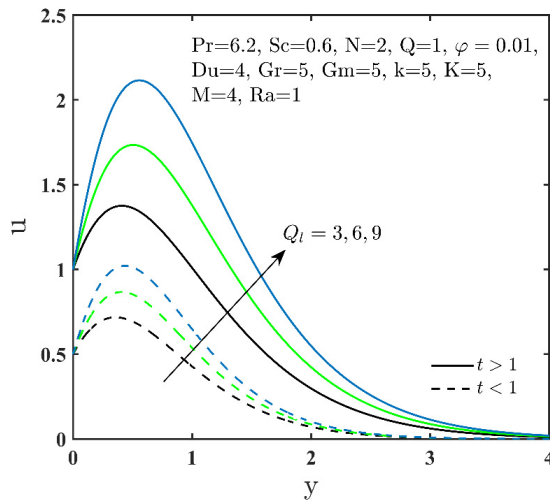


Fig. 5. (Color online) Velocity layout for Q_l .

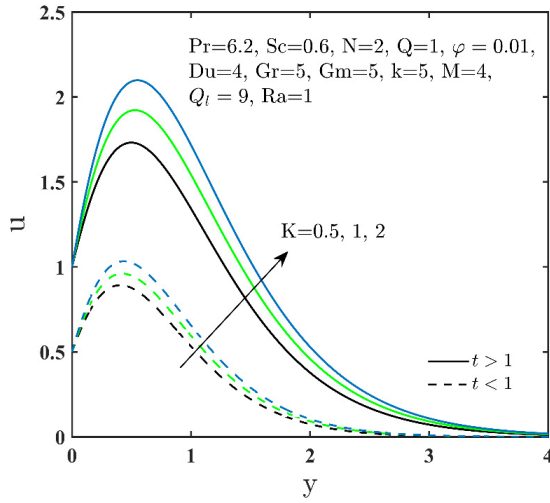


Fig. 6. (Color online) Velocity layout for K .

reducing the viscosity. That is fluid moves faster for small viscosity, which is physically true in nature.

Figure 8 shows that the diffusion-thermo effect enlarges the thermal frontier layer thickness. Reducing in Du retards the influences of the concentration gradients on the temperature distributions. Thus, the magnitude of the temperature is reduced, which leads to a cooling of the frontier layer. Figure 9 elucidates that temperature enhances with increasing heat source (Q). It is because energy is lost for greater exposure to heat and thus temperature layer is lifted. The enlargement of temperature distribution under the consequence of the absorption radiation parameter (Q_l)

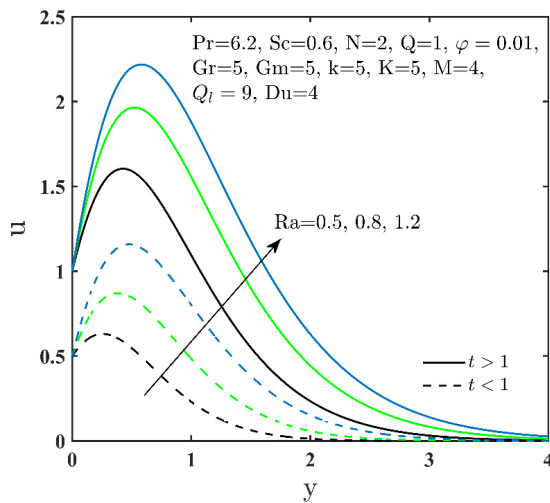


Fig. 7. (Color online) Velocity layout for Ra .

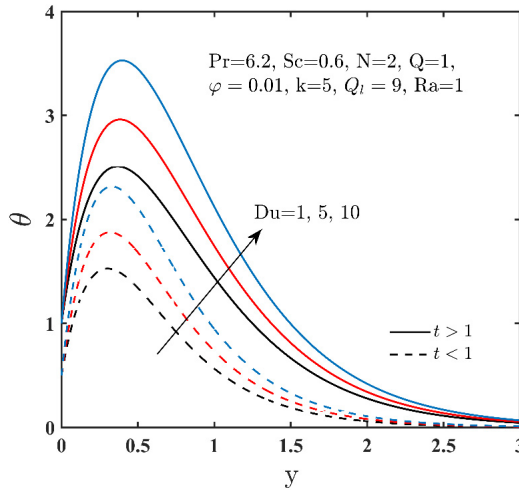


Fig. 8. (Color online) Temperature layout for Du .

is delineated in Fig. 10. This is because as heat is absorbed, buoyant force stimulates the flow temperature all over the fluid domain. It is clear that non-dimensional temperature is an expanding function of radiation absorption. This is because once heat is absorbed, buoyant force rushes the flow. In contrast, for thermal radiation (N), Fig. 11 demonstrates the opposite phenomenon. It is because the heat from the fluid region is radiated outward in the form of thermal radiation, which lowers the temperature profile. In the actual world, this is exactly how things work.

Figures 12 and 13 highlight the behavior of concentration profiles for isothermal and ramped cases, respectively, with dissimilar values of chemical reaction

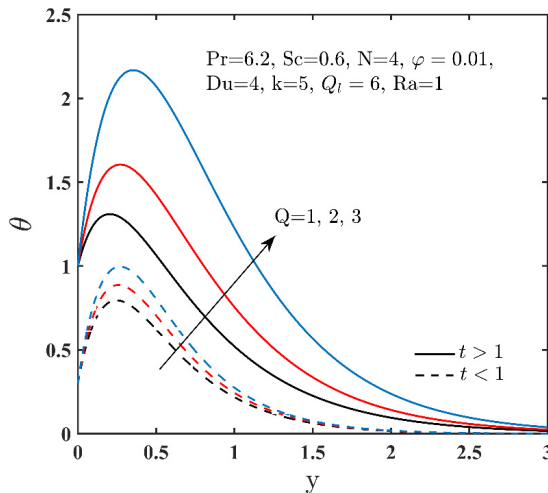


Fig. 9. (Color online) Temperature layout for Q .

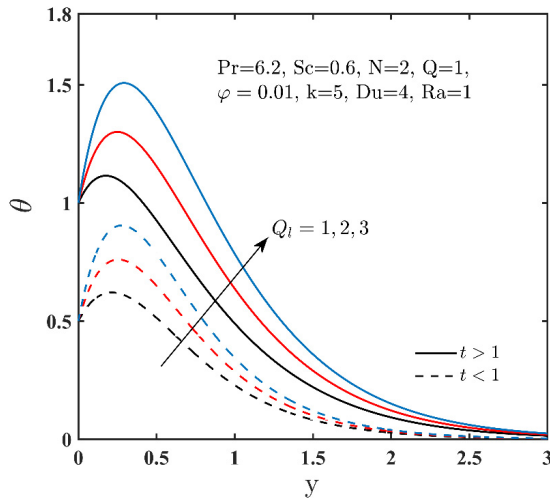


Fig. 10. (Color online) Temperature layout for Q_i .

parameter (k). It can be spotted that increasing chemical reactions drastically diminishes the concentration profile. The basis of this change is that the number of dissolved particles exposed to the action of the chemical reaction effect expands as chemical reaction parameter increases, causing a reduction in the thickness of the concentration boundary layer. This result is consistent with physical realities and also agrees excellently with the investigation of Kataria and Patel.³⁷

Computational outcomes of the shear stress τ at the plate $y = 0$ for multiple values of Du, Q_i, Ra, Q, M, K and φ are presented in Table 2. Table 2 manifests that due to the fluid movement, frictional resistance at the plate increases with an

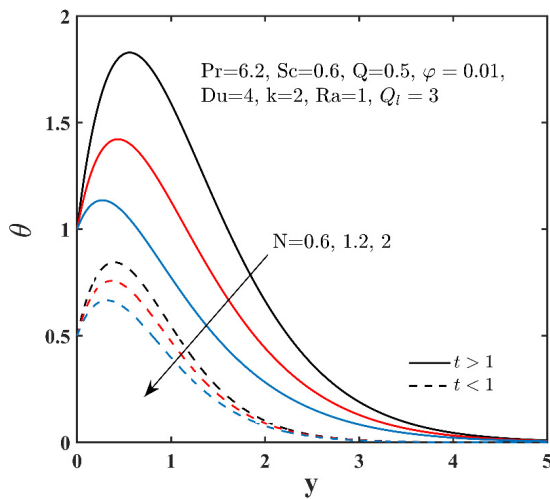


Fig. 11. (Color online) Temperature layout for N .

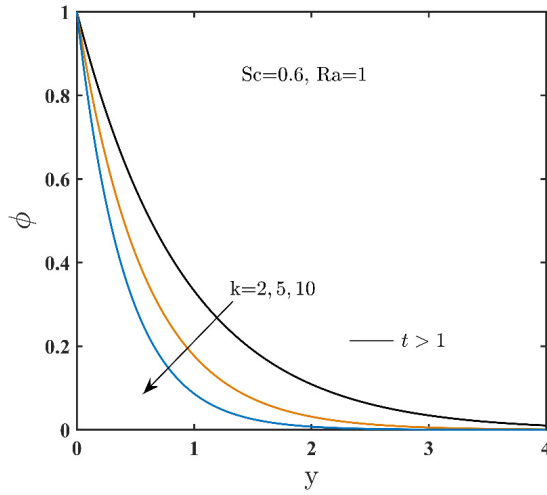


Fig. 12. (Color online) Concentration layout for k ($t > 1$).

increment in Du , Q_l , Q and K whereas a converse phenomenon is perceived for Ra , M and φ as visible in Table 2. Table 3 is drawn to scrutinize the behavior of heat transfer rate under the impact of Du , Ra , Q , Q_l and k . It is evident that the rate of heat transfer is enhanced due to an augmentation in all these parameters.

Surface plots are a type of three-dimensional data visualization. Instead of displaying individual data points, surface plots show the functional relation between a dependent variable and two independent variables. Figures 14–16 represent surface plots for Nusselt number and Sherwood number for different flow parameters. It is apparent from Fig. 14 that the Nusselt number gets enhanced for higher values of

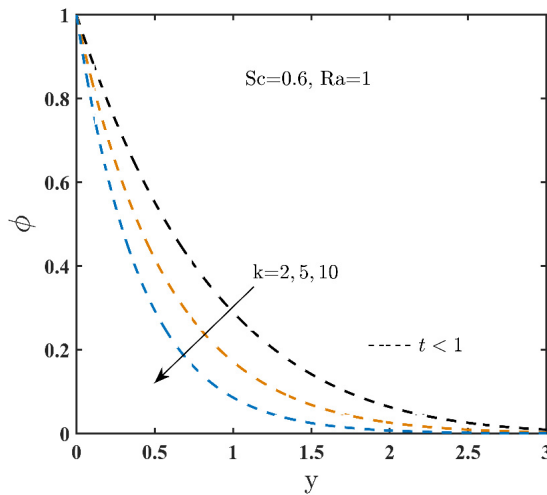


Fig. 13. (Color online) Concentration layout for k ($t < 1$).

Table 2. Skin friction (shear stress) when $Pr = 6.2$, $Sc = 0.6$, $N = 5$, $Gm = 5$, $Gr = 5$, $k = 1$.

Du	Q_l	Ra	Q	M	K	φ	τ	
							($t = 0.5$)	($t = 1.5$)
1	5	5	1	5	5	0.01	2.0021	1.1919
2	—	—	—	—	—	—	2.0259	1.2152
3	—	—	—	—	—	—	2.0496	1.2384
4	—	—	—	—	—	—	2.0734	1.2616
5	1	—	—	—	—	—	1.1156	0.3248
—	2	—	—	—	—	—	1.3610	0.5648
—	3	—	—	—	—	—	1.6064	0.8048
—	4	—	—	—	—	—	1.8518	1.0448
—	5	1	—	—	—	—	2.3208	1.4421
—	—	2	—	—	—	—	2.2447	1.3130
—	—	3	—	—	—	—	2.1684	1.2900
—	—	4	—	—	—	—	2.1214	1.2857
—	—	5	0.5	—	—	—	1.9667	1.1421
—	—	—	1.5	—	—	—	2.2569	1.4588
—	—	—	2.5	—	—	—	2.7188	1.9589
—	—	—	3.5	—	—	—	3.5549	2.9076
—	—	—	1	1	—	—	4.9661	4.9285
—	—	—	—	2	—	—	3.8588	3.4513
—	—	—	—	3	—	—	3.0753	2.5199
—	—	—	—	4	—	—	2.5221	1.8330
—	—	—	—	5	1	—	1.8174	0.9138
—	—	—	—	—	2	—	1.9872	1.1400
—	—	—	—	—	3	—	2.0475	1.2196
—	—	—	—	—	4	—	2.0784	1.2602
—	—	—	—	—	5	0.1	1.4853	0.3997
—	—	—	—	—	—	0.2	0.7387	-0.7776
—	—	—	—	—	—	0.3	-0.1724	-2.3256
—	—	—	—	—	—	0.4	-1.4050	-4.5425

Table 3. Nusselt number (rate of heat transfer) when $Pr = 6.2$, $Sc = 0.6$, $\varphi = 0.01$, $N = 2$.

Du	Ra	Q	Q_l	k	Nu	
					($t = 0.5$)	($t = 1.5$)
1	0.5	1	3	1	0.1814	1.6905
2	—	—	—	—	0.4416	1.8926
3	—	—	—	—	0.7019	2.0947
4	—	—	—	—	0.9621	2.2968
—	0.5	—	—	—	0.9621	2.2968
—	0.8	—	—	—	1.9981	3.0722
—	1.2	—	—	—	2.8414	3.5450
—	1.5	—	—	—	3.2736	3.7201
—	0.5	0.2	—	—	0.8353	1.2689
—	—	0.4	—	—	0.9089	1.5526
—	—	0.8	—	—	0.9898	2.0882
—	—	1.2	—	—	1.0721	2.6585

Table 3. (Continued)

Du	Ra	Q	Q _l	k	Nu	Nu
					(t = 0.5)	(t = 1.5)
—	—	1	4	—	1.9629	3.7949
—	—	—	5	—	2.9638	5.2929
			6		3.9646	6.7910
			7		4.9654	8.2890
—	—	—	3	2	1.2426	2.5888
—	—	—	—	3	1.5198	2.8861
				4	1.7925	3.1838
				5	2.0607	3.4799

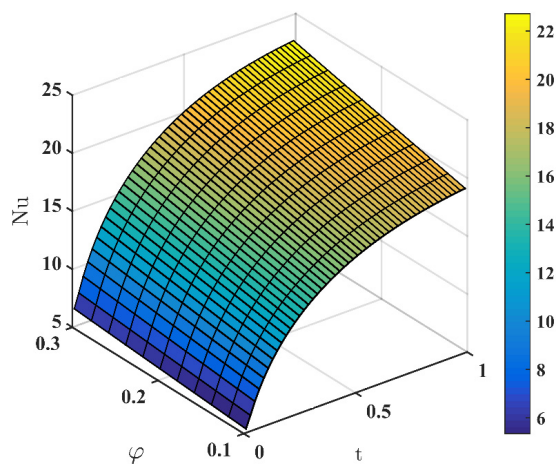


Fig. 14. (Color online) Surface plot of the rate of heat transfer for φ .

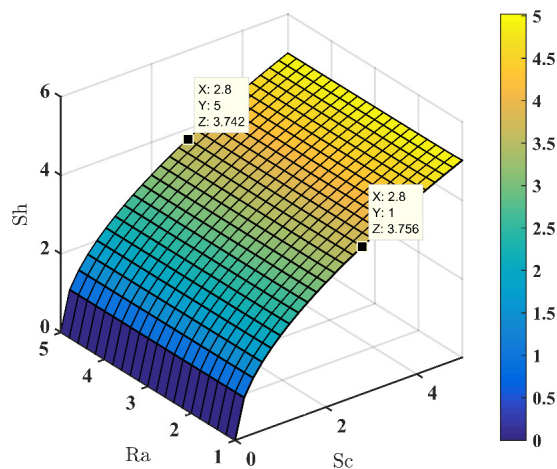


Fig. 15. (Color online) Surface plot of the rate of mass transfer for Ra.

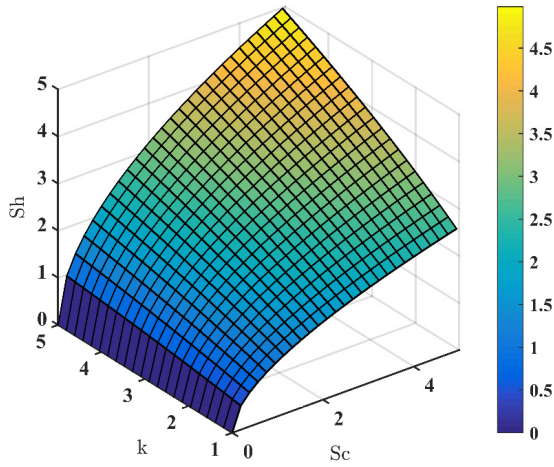


Fig. 16. (Color online) Surface plot of the rate of mass transfer for k .

volume concentration of nanoparticles φ . So, it can be concluded that the rate of heat transfer is an increasing function of φ . The behavior of mass transfer rate for ramped parameter Ra and chemical reaction k has been plotted in Figs. 15 and 16. These figures reveal that the mass transfer coefficient for ramped parameter Ra decreases while it hikes upon increment of chemical reaction effect k .

6. Comparison and Validation of Results

One of the present outcomes for a particular case is compared with the work of Krishna *et al.*³⁸ to check the accuracy of our findings. Concentration profiles with $k = 0, Ra = 1$ are displayed in Figs. 17 and 18. Figures 17 and 18 have been compared with Figs. 14(a) and 14(b) of Krishna *et al.*,³⁸ respectively. Both figures

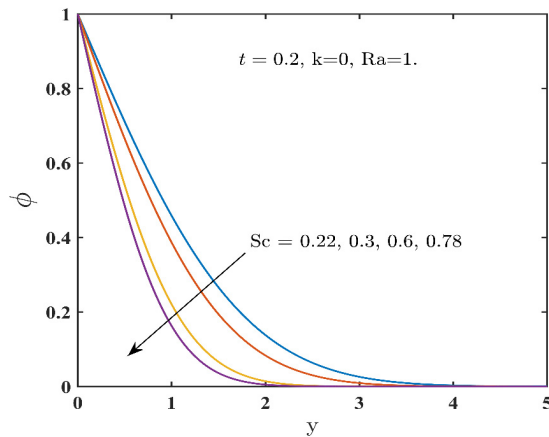


Fig. 17. (Color online) Comparison of concentration profile with Veera Krishna *et al.*³⁸ for Sc .

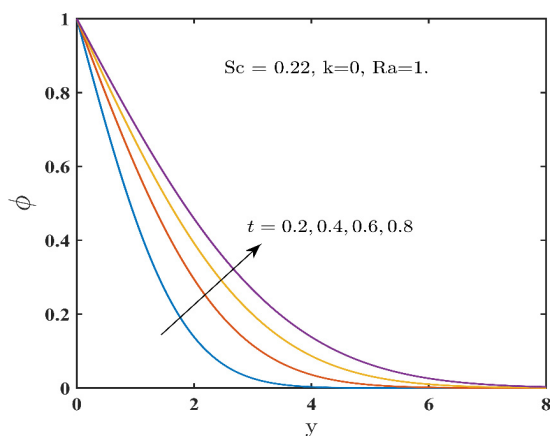


Fig. 18. (Color online) Comparison of concentration profile with Veera Krishna *et al.*³⁸ for t .

Table 4. Comparison of results for concentration.

y	t	Sc	ϕ	
			Previous work of Veera Krishna <i>et al.</i> ³⁸	Present work with $k = 0, Ra = 1$.
0.2	0.2	0.22	0.8821	0.8821
0.4			0.7667	0.7667
0.6			0.6563	0.6563
0.8			0.5530	0.5530
—	0.4	—	0.6748	0.6748
	0.6		0.7319	0.7319
	0.8		0.7667	0.7667
—	—	0.30	0.7290	0.7290
		0.60	0.6242	0.6242
		0.78	0.5765	0.5765

uniquely establish the fact that the Sherwood number lessens with growing Sc and enlarges with escalating time throughout the fluid region. Further, the authors calculated the numerical values for the concentration profile of the work of Krishna *et al.*³⁸ for different parameters and compared it with the present work with $k = 0$ and $Ra = 1$, which is presented in Table 4. It is observed that the numerical values for the two models are exactly identical. It is clear from these comparisons that there is excellent agreement among the numerical and graphical solutions, which validates the accuracy and validity of the solution obtained using the present method.

7. Conclusions

The core interest of this scrutiny is on the convective hydromagnetic flow of Cu-water nanofluid with diffusion-thermo effect, radiative absorption, and heat generation when ramping wall velocity and temperature are applied simultaneously.

Some remarkable findings are summarized as follows:

- Concentration, temperature and velocity profiles in case of ramped conditions are less than in isothermal conditions.
- Velocity and temperature profile enhance due to the amplification of Dufour as well as radiation absorption parameter.
- Fluid becomes hot for increasing heat source parameter.
- Chemical reaction parameter declines the solutal boundary layer drastically.
- Intensification of the Dufour parameter and radiation absorption leads to an increase in the resistive force at the plate.
- Heat transfer rate is amplified by the ramped parameter, whereas the mass transfer rate is affected in the opposite way.
- Volume concentration of nanoparticles has a tendency to augment the heat transmission rate.

Appendix A

$$f(\xi, a, y, t) = \left(\frac{t}{2} + \frac{y\sqrt{\xi}}{4\sqrt{a}}\right) e^{y\sqrt{\xi a}} \operatorname{erfc}\left(\frac{y\sqrt{\xi}}{2\sqrt{t}} + \sqrt{at}\right) + \left(\frac{t}{2} - \frac{y\sqrt{\xi}}{4\sqrt{a}}\right) e^{-y\sqrt{\xi a}} \times \operatorname{erfc}\left(\frac{y\sqrt{\xi}}{2\sqrt{t}} - \sqrt{at}\right), \quad (\text{A.1})$$

$$\psi(\xi, a, y, t) = \frac{1}{2} \left[e^{\sqrt{\xi a} y} \operatorname{erfc}\left(\frac{\sqrt{\xi} y}{2\sqrt{t}} + \sqrt{at}\right) + e^{-\sqrt{\xi a} y} \operatorname{erfc}\left(\frac{\sqrt{\xi} y}{2\sqrt{t}} - \sqrt{at}\right) \right]. \quad (\text{A.2})$$

Appendix B

The “bar” function that is used in Sec. 3 is defined as follows: for any function $h(a, b, y, t)$, $\bar{h} = h(a, b, y, t - 1)H(t - 1)$.

$$H(t - 1) = \operatorname{heaviside}(t - 1) = \begin{cases} 0, & t < 1, \\ \frac{1}{2}, & t = 0, \\ 1, & t > 1. \end{cases}$$

References

1. S. U. S. Choi, *Proc. ASME Int. Mech. Eng. Congress Expo.* **66**, 99 (1995).
2. M. A. Ahmed et al., *Case Stud. Therm. Eng.* **4**, 65 (2014).
3. J. Buongiorno, *J. Heat Trans.* **128**, 240 (2006).
4. S. K. Das et al., *J. Heat Trans.* **125**, 567 (2003).
5. M.-S. Liu et al., *Chem. Eng. Technol.* **29**, 72 (2006).
6. J. A. Eastman et al., *Appl. Phys. Lett.* **78**, 18 (2001).
7. X. Wang, X. Xu and S. U. S. Choi, *J. Thermophys. Heat Trans.* **13**, 474 (1999).

8. S. Lee *et al.*, *J. Heat Trans.* **121**, 280 (1999).
9. D. Wen and Y. Ding, *J. Thermophys. Heat Trans.* **18**, 481 (2004).
10. M. A. A. Hamad, I. Pop and A. I. M. Ismail, *Nonlinear Anal. Real World Appl.* **12**, 1338 (2011).
11. S. Das and R. N. Jana, *Alex. Eng. J.* **54**, 55 (2015).
12. G. S. Seth and M. K. Mishra, *Adv. Powder Technol.* **28**, 375 (2017).
13. M. V. Krishna, N. A. Ahamad and A. J. Chamkha, *Ain Shams Eng. J.* **12**, 3043 (2021).
14. P. D. Prasad, R. K. Kumar and S. V. K. Varma, *Ain Shams Eng. J.* **9**, 801 (2018).
15. B. Mahanthesh, B. J. Gireesha and R. S. R. Gorla, *Alex. Eng. J.* **55**, 569 (2016).
16. A. J. Chamkha and A. M. Aly, *Chem. Eng. Commun.* **198**, 425 (2010).
17. M. Turkyilmazoglu and I. Pop, *Int. J. Heat Mass Trans.* **59**, 167 (2013).
18. M. Sheikholeslami *et al.*, *J. Magn. Magn. Mater.* **374**, 36 (2015).
19. N. A. Ahamad, M. V. Krishna and A. J. Chamkha, *J. Nanofluids.* **9**, 177 (2020).
20. P. S. Reddy and A. J. Chamkha, *Adv. Powder Technol.* **27**, 1207 (2016).
21. T. Hayat *et al.*, *J. Mol. Liq.* **220**, 693 (2016).
22. A. K. Singha *et al.*, *J. Nanofluids.* **10**, 506 (2021).
23. I. Waini, A. Ishak and I. Pop, *Int. J. Numer. Methods Heat Fluid Flow.* **31**, 766 (2020).
24. D. Pal, G. Mandal and K. Vajravalu, *Appl. Math. Comput.* **287**, 184 (2016).
25. N. Ahmed and M. Dutta, *Int. J. Phys. Sci.* **8**, 254 (2013).
26. T. Anwar, P. Kumam and W. Watthayu, *Sci. Rep.* **10**, 17830 (2020).
27. S. I. Abdelsalam, K. S. Mekheimer and A. Z. Zaher, *Chin. J. Phys.* **67**, 314 (2020).
28. K. S. Mekheimer, A. M. Salem and A. Z. Zaher, *Chin. J. Phys.* **51**, 968 (2013).
29. K. S. Mekheimer, A. M. Salem and A. Z. Zaher, *J. Egypt. Math. Soc.* **22**, 143 (2014).
30. A. Q. El Idrissi, E. G. da Silva and D. Zeidan, *Ann. Nucl. Energy.* **182**, 109578 (2023).
31. D. Zeidan *et al.*, *Int. J. Numer. Methods Fluids* **95**, 242 (2023).
32. D. Zeidan, L. T. Zhang and E. Goncalves, *Int. J. Appl. Mech.* **12**, 2050049 (2020).
33. B. K. Sharma *et al.*, *Int. J. Mod. Phys. B.* **37**, 2350095 (2022).
34. A. Shahid *et al.*, *Sustainable Energy Technol. Assess.* **52**, 102029 (2022).
35. A. C. Cogley, W. G. Vincent and S. E. Gilles, *AIAA J.* **6**, 551 (1968).
36. Y. X. Li *et al.*, *Alex. Eng. J.* **61**, 2484 (2022).
37. H. R. Kataria and H. R. Patel, *Alex. Eng. J.* **57**, 73 (2018).
38. M. V. Krishna, N. A. Ahamad and A. J. Chamkha, *Ain Shams Eng. J.* **12**, 3043 (2021).